OPEN ACCESS
JOURNAL OF ADVANCED DIELECTRICS
Vol. 10, No. 6 (2020) 2050029 (16 pages)

DOI: 10.1142/S2010135X20500290

Electrocaloric devices part II: All-solid heat pump without moving parts

Farrukh Najmi*, Jianping He†, Lorenzo Cremaschi‡ and Z.-Y. Cheng*,§
*Materials Research and Education Center
Auburn University, Auburn, AL 36849, USA
†School of Materials Engineering
Shanghai University of Engineering Science
Shanghai 201620, P. R. China
‡Department of Mechanical Engineering
Auburn University, Auburn, AL 36849, USA
§chengzh@eng.auburn.edu

Received 13 August 2020; Revised 9 October 2020; Accepted 26 October 2020; Published 16 December 2020

Various designs have been introduced to build heat pumps using the electrocaloric effect (ECE). Each of all the current designs uses at least one moving part, which significantly reduces the reliability of the pump and adds complexities. In this work, a new all-solid design is introduced, in which two layers of an electrocaloric material (ECM) are permanently sandwiched in the source and sink, which would significantly increase the device's reliability since nothing moves and all are permanently bound together. More importantly, the electric fields applied on two ECM layers are independently controlled. A special sequence for the electric fields on two ECM layers is introduced. Numerical calculation was used to simulate the device's performance by using the newly introduced analytical solutions for the heat conduction in the system. It is concluded that a continuous heat transformation from the source to sink at the same temperature can be achieved when the contacting coefficient, $K_\varepsilon = \sqrt{(k^c\rho^c c_p^c)/(k^o\rho^o c_p^o)}$, is very small, where k, ρ, and c_p are thermal conductivity, density, and heat capacity, respectively, while the superscript c and o represent the ECM and source/sink, respectively.

Keywords: Electrocaloric based heat pump; electrocaloric effect; numerical calculation.

1. Introduction

Vapor-compression (VC) refrigeration has served as a workhorse technology for more than a century in heat pumping, refrigerating, and air-conditioning applications. However, the VC is one of the sources responsible for global warming gases.[1,2] Additionally, the VC refrigeration is bulky, which limits its capability in miniaturization. On the other side, due to the increasing usage of electronics in our daily life, cooling of electronic components, such as IC chips, becomes more and more important. It remains a challenge in the development of miniaturized refrigeration for the electronic devices and systems. Therefore, it is highly desirable to develop alternative technologies to replace the VC refrigeration.

Regarding the alternative technologies, in the 1994 Canada convention about 12 not-in-kind (NIK) technologies were considered to be the potential candidates for next generation cooling, refrigeration, and/or heat pumping applications.[3] Tremendous scientific efforts to explore these potential candidates have been carried out. Solid state cooling systems based on magnetocaloric effect (MCE)[4] and thermoelectric effect (TE), have been successfully developed and commercialized. MCE-based systems were successfully developed for several cryogenic applications, but the involvement of high magnetic fields has always been an issue and hindered their scalability.[5] On the other hand, TE-based coolers offer advantages of small-scale manufacturing, flexibility, silent operation (no moving parts) and durability. A main disadvantage associated with TE-based device is heat generation due to conduction,[6] poor efficiency, and high manufacturing costs.[7]

The electrocaloric effect (ECE) is a coupling effect between the thermal and electrical energy in the dielectrics with 1 of 10 polar structures. A dielectric with a useful ECE is also named as an electrocaloric material (ECM). Due to the ECE, the temperature of an ECM can be changed reversibly by the electric field. Therefore, the ECE was perceived highly as an attractive candidate for future solid-state cooling technologies[3,4,8] and has been considered as a potential alternative of VC technology due to its efficiency near to Carnot cycle.[9] Some scientific efforts to exploit ECE for solid-state cooling and refrigeration were carried out in the last decades of the 20th century.[10] Due to the low electrocaloric coupling coefficients (i.e., the temperature change induced by the electric field is less than 1K)[4,11] of then known ECMs; however, they could not get much attention of research community.

In 2006 and 2008, when a giant electrocaloric coefficient was observed in PZT thin films and PVDF polymer film, respectively,[12,13] ECE again received attention and triggered the research community to explore the ECE in the next generation cooling devices. An avalanche of research publications is observed in which various ECMs (i.e., both ferroelectrics and relaxor ferroelectrics) including ceramics, single crystals, and polymer films were investigated to achieve a high temperature change (ΔT_{EC}) in an ECM due to the change in the external electric field.[11,12,14–18] The observed ΔT_{EC} is dependent on the electric field as[9]:

$$\Delta T_{EC} \cong -\frac{T}{\rho c^{E,X}} \int_{E_1}^{E_2} \left(\frac{\partial D}{\partial T}\right)_E dE, \tag{1}$$

where T is the temperature, E_1 and E_2 are starting and ending electric fields applied on the ECM, respectively, D is the electric displacement induced in the ECM, $c^{E,X}$ is the heat capacity at constant electric field and stress, and ρ is the mass density of the ECM. In Eq. (1), the approximation was used since both ρ and $c^{E,X}$ are treated as constants, but these material properties are dependent on the temperature.[19] A ΔT_{EC} as high as 4.5°C in modified barium titanate (BZT) ceramics,[14] 53.8°C in PLZST thick films[20] and 45.3°C in thin films of relaxor PBZ[21] have been reported. The detailed information about these newly developed high-performance ECMs can be found in some recently published review articles.[11,22–24]

Regarding ECE-based heat pumps or cooling devices, various innovative designs have been conceptualized, analyzed, prototyped, and published over the past decade to achieve directional heat flow.[25] The working principle of most of these reported devices is based on the concept of active electrocaloric regenerator (AER) — an adaptation of active magnetocaloric regeneration (AMR).[4] ECE-based device was first demonstrated using AER.[10] In an AER, the ECM is used as both a refrigerant and regenerator (that is why the term *Active*)[4] and a liquid is used as a working material to transfer thermal energy from cold end to hot end through the porous structure of AER. A reverse Bryton cycle[26,27] — *having two adiabatic and two isofield cycles* — is applied on the ECM. The temperature of ECM decreases/increases adiabatically during depolarization/polarization, respectively, whereas the heat is absorbed/rejected during the isofield cycles. Designs based on fluidic AER have been reported and demonstrated by several groups.[7,28–30] Despite the fact that it is the best-known approach, it offers limited efficiency due to convective heat coupling,[30] losses due to oscillatory fluid flow and reduced sealing reliability.[25] More importantly, it requires additional system to move the liquid. To avoid the usage of fluid, translational solid AER was introduced,[31] which overcomes the issues associated with fluidic AER devices.[32] Similarly, a design of using direct ECE through a rotational mechanism was introduced to build ECE regeneration without using any external regenerator.[33,34] These all-solid designs face some difficulties, like electrical insulation and low efficiency, due to solid-solid friction losses.[25] In other words, although these designs of ECE-based refrigeration offer some great advantages, they face some critical challenges associated with the usage of pumping mechanisms (fluidic AER) and mechanical actuation (all-solid AER) that result into complex designs and limit their scalability.

Some cascade prototypes, *without regeneration*, have been reported. For example, the electrostatic force has been exploited as the driving force for actuating ECM to achieve direct thermal coupling/decoupling between ECM and sink/source.[35,36] The electromechanical coupling effect was also used to actuate the ECM to achieve thermal coupling/decoupling between heat sink and heat source.[37] Like all-solid AER, all these designs use a physical movement of ECM to achieve a continuous heat flow along one direction. However, the usage of moving ECM in these designs creates a new challenge — thermal contact between different pieces of solid materials, such as perfectness of thermal contacts and high resistance of thermal interface, which may be strongly influenced by the time as the device continuously operates. This results in a critical concern — reliability of these devices due to thermal connection between different solid surfaces. To overcome this concern, liquid droplet has been used to improve the thermal contacts, in which a mechanical motorized mechanism is used to achieve alternative thermal coupling/decoupling.[38]

To avoid the usage of moving ECM, different heat switches have been used to control the direction of heat flow, such as liquid based heat switches by using high thermal anisotropic properties,[39] TE thin films as heat switches,[26,40,41] and motorized heat switches (i.e., thin silicon sheets having silicon oil in between) with a high thermal contrast ratio up to 27.[42] Unfortunately, the heat switches face some critical challenges, such as limited thermal contrast ratio from the anisotropic properties, high cost and parasitic losses due to joule heating in TE-based switches, and involvement of motorized actuation mechanism. Additionally, the usage of the heat switches limits the performance of ECE-based devices due to limited switching frequency and small conductivity ratio.[25]

A concept of all solid (i.e., complete solid state) cooling line — *without involvement of any regenerator, mechanical actuators, and/or thermal switches* — has been reported. In one design, asymmetric boundary conditions — one end is thermally isolated and the other end is kept at a constant temperature[43–46] — is used to achieve temperature gradient along the line. In another design, kinetics control of ECE by controlling the rising and falling electric field rates was exploited to create a temperature gradients at two sides of ECMs.[47] There is a critical issue that all these designs of all-solid cooling line have not documented whether they can achieve a continuous cooling/heat pumping operation[11] or it is just a temperature redistribution in the cooling line. In summary, although a great progress has been made in the development of high-performance ECM and many designs of ECE-based device have been introduced, there is not a design/system of ECE-based cooling line that does not use other mechanisms (i.e., actuators for moving part, technologies for

heat switches, etc.). The usage of other mechanisms increases the complexity of the device and reduces their miniaturization capability.

Here, in this work, a multilayer design of all-solid ECE-based cooling line is introduced. In this design, double layers of an ECM are used, and no moving part or heat switch is employed. The operation principle of the design is based on independent electric field applied on each of two ECM layers and a special pattern (i.e., a three-step process) of the electric field on these two ECM layers. Numeric calculation based on the analytical solution[48] is carried out to determine the heat flow in the multilayer structure. It is demonstrated that the design can achieve a continuous heat flow along one direction between two bodies at the same temperature.

2. Model and Working Principle

The multilayer structure is shown in Fig. 1, where two semi-infinite layers on left and right represent the heat sink (SI) and heat source (SO), respectively, while two layers (EC1 and EC2) of an ECM are sandwiched into the SI and SO. All four bodies/layers are permanently bonded together, and nothing moves. That is, in this all-solid design, neither moving part nor actuator, nor heat switch is used. Therefore, a high reliability is expected.

Considering the case that all bodies reach a thermal equilibrium state (i.e., at the same temperature T), and then a three-step electric field cycle as shown in Fig. 3, and Fig. 3 is applied on the two ECM layers. Assume that the change in the electric field is so fast that the temperature change in the ECM layer due to the ECE can be treated as an adiabatic process, which is as exactly what has been observed and used in ECE-based devices.[43,46]

The details about the three-step process/cycle are:

Step-I: The electric field on both EC1 and EC2 is changed so that the temperature of EC1 increases by $\Delta T(>0)$ and the temperature of EC2 decreases by ΔT; and then the electric field on both EC1 and EC2 is kept for a certain time to allow the temperature in all four bodies reaches their new thermal equilibrium state (i.e., the same temperature T) due to the heat conduction. During Step-I, it is expected that a certain amount of heat ($Q^{\mathrm{I}}_{\mathrm{SO}}$) will be transferred from right (SO) to EC2 and a certain amount of heat ($Q^{\mathrm{I}}_{\mathrm{SI}}$) will be transferred from EC1 to left (SI) as shown in Fig. 2.

Step-II: The electric field on EC2 is still kept as it is in Step-I, but the electric field on EC1 is changed so that the temperature of the EC1 is decreased by ΔT, and then the electric field on EC1 and EC2 is kept to allow the system reach their thermal equilibrium state (i.e., the same temperature T) again due to the thermal conduction. During Step-II, it is expected that a certain amount of heat ($Q^{\mathrm{II}}_{\mathrm{SO}}$) will be transferred from right (SO) to EC2 and a certain amount of heat ($Q^{\mathrm{II}}_{\mathrm{SI}}$) will be transferred from left (SI) to EC1 as shown in Fig. 2.

Step-III: The electric field on EC1 is kept as it is in Step-II, but the electric field on EC2 is changed so that the temperature of EC2 is increased by ΔT, and then it is kept to allow four bodies to reach their thermal equilibrium state (i.e., the same temperature T) again. During Step-III, it is expected that a certain amount of heat ($Q^{\mathrm{III}}_{\mathrm{SO}}$) will be transferred from EC2 to right (SO) and a certain amount of heat ($Q^{\mathrm{III}}_{\mathrm{SI}}$) will be transferred from EC1 to left (SI) as shown in Fig. 2.

The change in the electric field on both EC1 and EC2 is schematically shown in Fig. 3 in order to achieve the thermal process shown in Fig. 2. Clearly, after one cycle (i.e., Step-I, Step-II and Step-III), the electric field on both EC1 and EC2

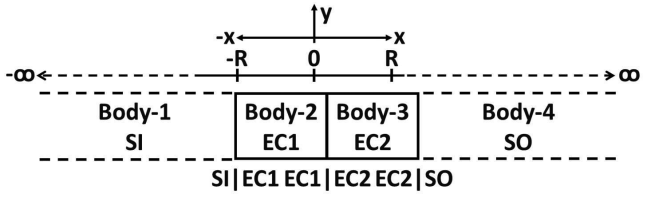

Fig. 1. Conceptual model of present EC heat pump.

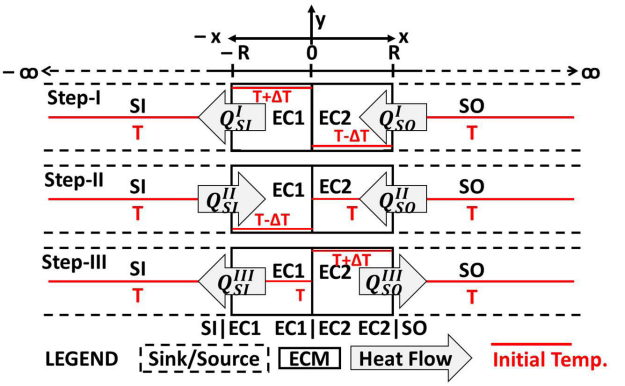

Fig. 2. Operational process of the three-step cycle for the system shown in Fig. 1.

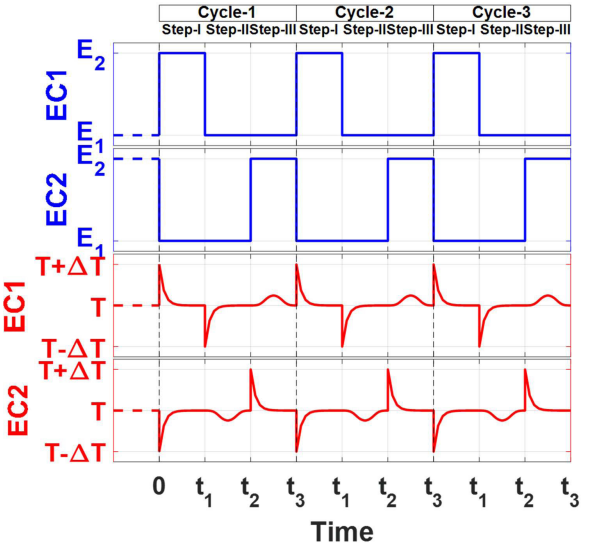

Fig. 3. Electric field cycle and corresponding temperature variations at the center of EC1 and EC2 (three cycles shown).

restores its original condition. In other words, the three-step process shown in Fig. 3 is repeatable. That is, the three-step process can be continuously repeated. Therefore, if a certain amount of heat can be transferred from right (SO) to left (SI) during one cycle of the three-step process, a continuous heat flow from SO to SI can be achieved. That is, a continuous heat flow from one body (SO) to the other (SI) can be achieved even two bodies are at the same temperature.

Regarding the heat flow during one cycle of the three-step process, as shown in Fig. 2, there will be an amount of heat (Q) transferred from SO to EC2 as: $Q = -Q^{\mathrm{I}}_{\mathrm{SO}} - Q^{\mathrm{II}}_{\mathrm{SO}} + Q^{\mathrm{III}}_{\mathrm{SO}}$. Similarly, there will be the same amount of heat transferred from EC1 to SI as: $Q = -Q^{I}_{\mathrm{SI}} + Q^{\mathrm{II}}_{\mathrm{SI}} - Q^{\mathrm{III}}_{\mathrm{SI}}$. That is, during one cycle of the three-step process, an amount of heat (Q) is transferred from right (SO) to left (SI), even though both SO and SI have the same temperature. Since the three-step process shown in Fig. 2 can be repeated as shown in Fig. 3, a continuous heat flow from SO (right) to SI (left) can be achieved by continuously repeating the process shown in Fig. 2. That is, a constant heat flow from SO to SI is expected, although both SO and SI have the same temperature.

First of all, let us assume all four bodies are exactly the same material, the heat conduction during Step-II and Step-III becomes a classic heat conduction problem[49]: an infinite plate with a finite uniform thickness is sandwiched into two semi-infinite media on both two sides of the plate. For this case, it is well known: $Q^{\mathrm{II}}_{\mathrm{SO}} = Q^{\mathrm{II}}_{\mathrm{SI}}$ and $Q^{\mathrm{III}}_{\mathrm{SO}} = Q^{\mathrm{III}}_{\mathrm{SI}}$. Based on the model shown in Fig. 2, one can get that $Q^{\mathrm{II}}_{\mathrm{SO}} = Q^{\mathrm{III}}_{\mathrm{SO}}$. Therefore, $Q^{\mathrm{II}}_{\mathrm{SO}} = Q^{\mathrm{II}}_{\mathrm{SI}} = Q^{\mathrm{III}}_{\mathrm{SO}} = Q^{\mathrm{III}}_{\mathrm{SI}}$. That is, $Q = Q^{I}_{\mathrm{SI}} = Q^{I}_{\mathrm{SO}}$. In other words, through one cycle of the three-step process illustrated in Fig. 2, the amount of heat (Q) transferred from right to left is only determined by Step-I.

It must be mentioned that during this three-step process, no movement of any part of the system is required and there are no other mechanisms involved. Only the thermal conduction among four bodies is involved. Since all four bodies are permanently bonded together, an excellent thermal contact can be achieved on three interfaces (SI|EC1, EC1|EC2, EC2|SO) and the thermal contact of these interfaces would not change with time. This is the principal advantage of the design introduced here over all reported ECE-based devices.

For the design introduced here, the key is that whether any heat transfers during the process or the Q is zero. If the Q is not zero, what is the condition (materials used for Body-1 to Body-4) to achieve a high Q and what is the time duration of each of these three steps? To answer these questions, numerical calculation is carried out.

3. Mathematical Model anD Analytical Solution

The unsteady heat equation (1D) for the four bodies can be written as in Eq. (2)[48,49]

$$\frac{\partial T_j(x,t)}{\partial t} = \alpha_j \frac{\partial^2 T_j(x,t)}{\partial x^2}, \tag{2}$$

where $T_j(x,t)(j = 1,2,3,4)$ are the temperatures at time t and location x in the body j: $\alpha_j = k_j/\rho_j c_{p_j}$ ($\mathrm{m^2 s^{-1}}$) are the thermal diffusivity of the body j, in which k_j ($\mathrm{Wm^{-1}K^{-1}}$), ρ_j ($\mathrm{kgm^{-3}}$), and c_{p_j} ($\mathrm{JK^{-1}kg^{-1}}$) are the thermal conductivity, mass density, and heat capacity, respectively, of the body j. In the heat pump model shown in Fig. 1, Body-2 and Body-3 are ECM bodies (EC1 and EC2) and they are the same, whereas Body-1 and Body-4 are SI and SO bodies and are the same. So, the following replacements may be made for simplification, $\alpha_2 = \alpha_3 = \alpha^c$ & $\alpha_1 = \alpha_4 = \alpha^o$, $k_2 = k_3 = k^c$ & $k_1 = k_4 = k^o$, $c_{p_2} = c_{p_3} = c_p^c$ & $c_{p_1} = c_{p_4} = c_p^o$ and $\rho_2 = \rho_3 = \rho^c$ & $\rho_1 = \rho_4 = \rho^o$, where superscripts represent center (EC1 and EC2) and outer bodies (SI and SO). The analytical solution for the time dependence of temperature profile in all four bodies was determined.[48] In the solution, following parameters were used: $K_\varepsilon = k^c/k^o\sqrt{\alpha^o/\alpha^c} = K_r/\sqrt{K_\alpha}(> 0)$ is referred to as contacting coefficient and characterizes the thermal activity of one body relative to other body,[49] $K_r = k^c/k^o$ is the relative thermal conductivity and $K_\alpha = \alpha^c/\alpha^o(> 0)$ is relative thermal inertia, $h = (1 - K_\varepsilon)/(1 + K_\varepsilon)$, $|h| < 1$. All $K_\varepsilon, h, K_\alpha$, and K_r are dimensionless.

3.1. *Initial conditions for thermal cycle*

The initial conditions for above mentioned steps (Step-I–Step-III) are given in Eqs. (3)–(5).

Step-I

$$\begin{array}{ll} T_{\mathrm{SI}}(x,0) = T_{\mathrm{SI},i} = T & -\infty < x < -R \\ T_{\mathrm{EC1}}(x,0) = T_{\mathrm{EC1},i} = T + \Delta T & -R < x < 0 \\ T_{\mathrm{EC2}}(x,0) = T_{\mathrm{EC2},i} = T - \Delta T & 0 < x < R \\ T_{\mathrm{SO}}(x,0) = T_{\mathrm{SO},i} = T & R < x < \infty \end{array} \tag{3}$$

Step-II

$$\begin{array}{ll} T_{\mathrm{SI}}(x,0) = T_{\mathrm{SI},i} = T & -\infty < x < -R \\ T_{\mathrm{EC1}}(x,0) = T_{\mathrm{EC1},i} = T - \Delta T & -R < x < 0 \\ T_{\mathrm{EC2}}(x,0) = T_{\mathrm{EC2},i} = T & 0 < x < R \\ T_{\mathrm{SO}}(x,0) = T_{\mathrm{SO},i} = T & R < x < \infty \end{array} \tag{4}$$

Step-III

$$\begin{array}{ll} T_{\mathrm{SI}}(x,0) = T_{\mathrm{SI},i} = T & -\infty < x < -R \\ T_{\mathrm{EC1}}(x,0) = T_{\mathrm{EC1},i} = T & -R < x < 0 \\ T_{\mathrm{EC2}}(x,0) = T_{\mathrm{EC2},i} = T + \Delta T & 0 < x < R \\ T_{\mathrm{SO}}(x,0) = T_{\mathrm{SO},i} = T & R < x < \infty \end{array} \tag{5}$$

3.2. *Temperature profiles*

The temperature profiles for all bodies (SI, EC1, EC2, and SO) involved in the system shown in Fig. 1 are determined in the previous work.[48] Here, the temperature profiles in SI and EC1 are given as a quick reference. The other information is presented in supplementary information as Eqs. (S.1) and (S.2).

3.2.1. Temperature profile of sink body

$$\begin{aligned}
&T_{\mathrm{SI}}(x,t) - T_{\mathrm{SI},i} \\
&\quad = \frac{K_\varepsilon}{1+K_\varepsilon}\Bigg\{(T_{\mathrm{EC1},i} - T_{\mathrm{SI},i})h\sum_{n=1}^{\infty} h^{2(n-1)} \\
&\qquad \times \operatorname{erfc}\frac{-x-R+(4n-0)K_\alpha^{-1/2}R}{2\sqrt{\alpha^o t}} \\
&\qquad - (T_{\mathrm{EC1},i} - T_{\mathrm{EC2},i})h\sum_{n=1}^{\infty} h^{2(n-1)} \\
&\qquad \times \operatorname{erfc}\frac{-x-R+(4n-1)K_\alpha^{-1/2}R}{2\sqrt{\alpha^o t}} \\
&\qquad - \frac{2(T_{\mathrm{EC2},i} - T_{\mathrm{SO},i})}{1+K_\varepsilon}\sum_{n=1}^{\infty} h^{2(n-1)} \\
&\qquad \times \operatorname{erfc}\frac{-x-R+(4n-2)K_a^{-1/2}R}{2\sqrt{\alpha^o t}} \\
&\qquad - (T_{\mathrm{EC1},i} - T_{\mathrm{EC2},i})\sum_{n=1}^{\infty} h^{2(n-1)} \\
&\qquad \times \operatorname{erfc}\frac{-x-R+(4n-3)K_\alpha^{-1/2}R}{2\sqrt{\alpha^o t}} \\
&\qquad + (T_{\mathrm{EC1},i} - T_{\mathrm{SI},i})\sum_{n=1}^{\infty} h^{2(n-1)} \\
&\qquad \times \operatorname{erfc}\frac{-x-R+(4n-4)K_\alpha^{-1/2}R}{2\sqrt{\alpha^o t}}\Bigg\} \qquad (6)
\end{aligned}$$

3.2.2. Temperature profile of EC1 body

$$\begin{aligned}
&T_{\mathrm{EC1}}(x,t) - T_{\mathrm{EC1},i} \\
&\quad = \frac{(T_{\mathrm{EC1},i} - T_{\mathrm{EC2},i})h^2}{2}\sum_{n=1}^{\infty} h^{2(n-1)} \\
&\qquad \times \operatorname{erfc}\frac{(4n-0)R+x}{2\sqrt{\alpha^c t}} + \frac{h}{1+K_\varepsilon}\sum_{n=1}^{\infty} h^{2(n-1)} \\
&\qquad \times \Big[(T_{\mathrm{EC1},i} - T_{\mathrm{SI},i}) \\
&\qquad \times \operatorname{erfc}\frac{(4n-1)R-x}{2\sqrt{\alpha^c t}} \\
&\qquad + (T_{\mathrm{EC2},i} - T_{\mathrm{SO},i}) \\
&\qquad \times \operatorname{erfc}\frac{(4n-1)R+x}{2\sqrt{\alpha^c t}}\Big] \\
&\qquad - \frac{h}{2}\sum_{n=1}^{\infty} h^{2(n-1)}\Big[(T_{\mathrm{EC1},i} - T_{\mathrm{EC2},i}) \\
&\qquad \times \operatorname{erfc}\frac{(4n-2)R-x}{2\sqrt{\alpha^c t}} - (T_{\mathrm{EC1},i} - T_{\mathrm{EC2},i}) \\
&\qquad \times \operatorname{erfc}\frac{(4n-2)R+x}{2\sqrt{\alpha^c t}}\Big] - \frac{1}{1+K_\varepsilon}\sum_{n=1}^{\infty} h^{2(n-1)} \\
&\qquad \times \Big[(T_{\mathrm{EC2},i} - T_{\mathrm{SO},i}) \\
&\qquad \times \operatorname{erfc}\frac{(4n-3)R-x}{2\sqrt{\alpha^c t}} \\
&\qquad + (T_{\mathrm{EC1},i} - T_{\mathrm{SI},i}) \\
&\qquad \times \operatorname{erfc}\frac{(4n-3)R+x}{2\sqrt{\alpha^c t}}\Big] \\
&\qquad - \frac{(T_{\mathrm{EC1},i} - T_{\mathrm{EC2},i})}{2}\sum_{n=1}^{\infty} h^{2(n-1)} \\
&\qquad \times \operatorname{erfc}\frac{(4n-4)R-x}{2\sqrt{\alpha^c t}} \qquad (7)
\end{aligned}$$

3.2.3. Heat flux through the interfaces

The heat flux (q) through the interfaces between the EC1 and SI (SI|EC1) and between the SO and EC2 (EC2|SO) has been determined in the previous work[48] and are given in supplementary information as Eqs. (S.3) and (S.4), respectively. The solution includes series with infinite terms as shown in Eqs. (S.3) and (S.4). It was proved that these series are convergent so that the sum of first N terms can be used as the summation of the series given in supplementary information.

The $N(\geq 4)$ used to calculate the sum of the series is calculated as,[48]

$$N = \frac{-\ln\delta - \ln(1-h^2\exp(-\gamma))}{\gamma - \ln h^2} \qquad (8)$$

where $\gamma = 12R^2/\alpha^c t(>0)$ and $\delta(0<\delta<<1)$ is the tolerance.

In Eq. (8), the tolerance δ is defined as the ratio of summation of all terms of series for $(n > N+1)$ to the value of first term only of the series. That is, the smaller the δ is, the closer are the results of Eqs. (S.3) and (S.4) to the real results. If Eq. (8) results in a number smaller than 4, $N = 4$ should be used.[48] In this paper, $\delta = 10^{-5}$ is used in all the calculations presented below. In other words, the uncertainty of the calculation is less than 0.001%.

3.2.4. Energy transfer through EC2|SO

The thermal energy passing through the interface EC2|SO per unit area is determined by integrating heat flux over the time spans by using the relation (9). For one complete three-step cycle, based on the first law of thermodynamics, one can get that the overall heat flows through SI|EC1 interface is the same as that through EC2|SO. Therefore, to determine the performance of the three-step cycle, one only needs to calculate the heat flows through EC2|SO that is shown in Eq. (10).

$$Q(t) = \int_0^t q(t)dt \qquad (9)$$

$$Q_{\mathrm{EC2|SO}} = \int_0^t q_{\mathrm{EC2|SO}}(t)dt$$

$$\begin{aligned}
Q_{\mathrm{EC2|SO}} = {} & \frac{2k^o}{\sqrt{\pi\alpha^o}} \frac{K_\varepsilon}{1+K_\varepsilon} \\
& \times \Bigg\{ (T_{\mathrm{EC2},i} - T_{\mathrm{SO},i}) h \sum_{n=1}^{N} h^{2(n-1)} \\
& \times \left[\sqrt{t} \exp\left(-\left[\frac{(4n-0)R}{2\sqrt{\alpha^c t}} \right]^2 \right) \right. \\
& \left. - \frac{(4n-0)R}{2\sqrt{\alpha^c}} \sqrt{\pi}\, \mathrm{erfc} \frac{(4n-0)R}{2\sqrt{\alpha^c t}} \right] \\
& + (T_{\mathrm{EC1},i} - T_{\mathrm{EC2},i}) h \sum_{n=1}^{N} h^{2(n-1)} \\
& \times \left[\sqrt{t} \exp\left(-\left[\frac{(4n-1)R}{2\sqrt{\alpha^c t}} \right]^2 \right) \right. \\
& \left. - \frac{(4n-1)R}{2\sqrt{\alpha^c}} \sqrt{\pi}\, \mathrm{erfc} \frac{(4n-1)R}{2\sqrt{\alpha^c t}} \right] \\
& - \frac{2(T_{\mathrm{EC1},i} - T_{\mathrm{SI},i})}{(1+K_\varepsilon)} \sum_{n=1}^{N} h^{2(n-1)} \\
& \times \left[\sqrt{t} \exp\left(-\left[\frac{(4n-2)R}{2\sqrt{\alpha^c t}} \right]^2 \right) \right. \\
& \left. - \frac{(4n-2)R}{2\sqrt{\alpha^c}} \sqrt{\pi}\, \mathrm{erfc} \frac{(4n-2)R}{2\sqrt{\alpha^c t}} \right] \\
& + (T_{\mathrm{EC1},i} - T_{\mathrm{EC2},i}) \sum_{n=1}^{N} h^{2(n-1)} \\
& \times \left[\sqrt{t} \exp\left(-\left[\frac{(4n-3)R}{2\sqrt{\alpha^c t}} \right]^2 \right) \right. \\
& \left. - \frac{(4n-3)R}{2\sqrt{\alpha^c}} \sqrt{\pi}\, \mathrm{erfc} \frac{(4n-3)R}{2\sqrt{\alpha^c t}} \right] \\
& + (T_{\mathrm{EC2},i} - T_{\mathrm{SO},i}) \sum_{n=1}^{N} h^{2(n-1)} \\
& \times \left[\sqrt{t} \exp\left(-\left[\frac{(4n-4)R}{2\sqrt{\alpha^c t}} \right]^2 \right) \right. \\
& \left. - \frac{(4n-4)R}{2\sqrt{\alpha^c}} \sqrt{\pi}\, \mathrm{erfc} \frac{(4n-4)R}{2\sqrt{\alpha^c t}} \right] \Bigg\} \qquad (10)
\end{aligned}$$

3.2.5. *Net heat energy transfer through the interface EC2|SO in one cycle*

As it has already been discussed that operation of the heat pump comprises of three steps, so the net energy through the interface EC2|SO may be determined using the initial conditions in Eq. (10). When the starting condition of each step is used, the general solution, Eq. (10) is further simplified as follows for each step.

1. Step-I

Using initial conditions (3) in Eq. (10), we get

$$\begin{aligned}
Q^I_{\mathrm{SO}} = {} & Q^I_{\mathrm{EC2|SO}} \\
= {} & \frac{2k^o}{\sqrt{\pi\alpha^o}} \frac{K_\varepsilon}{1+K_\varepsilon} \times \Bigg\{ (-\Delta T) h \sum_{n=1}^{N} h^{2(n-1)} \\
& \left[\sqrt{t} \exp\left(-\left[\frac{(4n-0)R}{2\sqrt{\alpha^c t}} \right]^2 \right) \right. \\
& \left. - \frac{(4n-0)R}{2\sqrt{\alpha^c}} \sqrt{\pi}\, \mathrm{erfc} \frac{(4n-0)R}{2\sqrt{\alpha^c t}} \right] \\
& + 2(\Delta T) h \sum_{n=1}^{N} h^{2(n-1)} \\
& \times \left[\sqrt{t} \exp\left(-\left[\frac{(4n-1)R}{2\sqrt{\alpha^c t}} \right]^2 \right) \right. \\
& \left. - \frac{(4n-1)R}{2\sqrt{\alpha^c}} \sqrt{\pi}\, \mathrm{erfc} \frac{(4n-1)R}{2\sqrt{\alpha^c t}} \right] \\
& - \frac{2(\Delta T)}{(1+K_\varepsilon)} \sum_{n=1}^{N} h^{2(n-1)} \\
& \times \left[\sqrt{t} \exp\left(-\left[\frac{(4n-2)R}{2\sqrt{\alpha^c t}} \right]^2 \right) \right. \\
& \left. - \frac{(4n-2)R}{2\sqrt{\alpha^c}} \sqrt{\pi}\, \mathrm{erfc} \frac{(4n-2)R}{2\sqrt{\alpha^c t}} \right] \\
& + 2(\Delta T) \sum_{n=1}^{N} h^{2(n-1)} \\
& \times \left[\sqrt{t} \exp\left(-\left[\frac{(4n-3)R}{2\sqrt{\alpha^c t}} \right]^2 \right) \right. \\
& \left. - \frac{(4n-3)R}{2\sqrt{\alpha^c}} \sqrt{\pi}\, \mathrm{erfc} \frac{(4n-3)R}{2\sqrt{\alpha^c t}} \right] \\
& + (-\Delta T) \sum_{n=1}^{N} h^{2(n-1)} \\
& \times \left[\sqrt{t} \exp\left(-\left[\frac{(4n-4)R}{2\sqrt{\alpha^c t}} \right]^2 \right) \right. \\
& \left. - \frac{(4n-4)R}{2\sqrt{\alpha^c}} \sqrt{\pi}\, \mathrm{erfc} \frac{(4n-4)R}{2\sqrt{\alpha^c t}} \right] \Bigg\} \qquad (11)
\end{aligned}$$

2. Step-II

Using initial conditions (4) in Eq. (10), we get

$$\begin{aligned}
Q^{\mathrm{II}}_{\mathrm{SO}} = {} & Q^{\mathrm{II}}_{\mathrm{EC2|SO}} \\
= {} & \frac{2k^o}{\sqrt{\pi\alpha^o}} \frac{K_\varepsilon}{1+K_\varepsilon} \times \Bigg\{ (-\Delta T) h \sum_{n=1}^{N} h^{2(n-1)} \\
& \times \left[\sqrt{t} \exp\left(-\left[\frac{(4n-1)R}{2\sqrt{\alpha^c t}} \right]^2 \right) \right. \\
& \left. - \frac{(4n-1)R}{2\sqrt{\alpha^c}} \sqrt{\pi}\, \mathrm{erfc} \frac{(4n-1)R}{2\sqrt{\alpha^c t}} \right]
\end{aligned}$$

$$
\begin{aligned}
&-\frac{2(-\Delta T)}{(1+K_\varepsilon)}\sum_{n=1}^{N} h^{2(n-1)} \\
&\times\left[\sqrt{t}\exp\left(-\left[\frac{(4n-2)R}{2\sqrt{\alpha^c t}}\right]^2\right)\right. \\
&\left.-\frac{(4n-2)R}{2\sqrt{\alpha^c}}\sqrt{\pi}\,\mathrm{erfc}\frac{(4n-2)R}{2\sqrt{\alpha^c t}}\right] \\
&+(-\Delta T)\sum_{n=1}^{N} h^{2(n-1)} \\
&\times\left[\sqrt{t}\exp\left(-\left[\frac{(4n-3)R}{2\sqrt{\alpha^c t}}\right]^2\right)\right. \\
&\left.-\frac{(4n-3)R}{2\sqrt{\alpha^c}}\sqrt{\pi}\,\mathrm{erfc}\frac{(4n-3)R}{2\sqrt{\alpha^c t}}\right]\Bigg\} \qquad (12)
\end{aligned}
$$

3. *Step-III*

Using initial conditions (5) in Eq. (10), we get

$$
\begin{aligned}
Q_{\mathrm{SO}}^{\mathrm{III}} &= Q_{\mathrm{EC2|SO}}^{\mathrm{III}} \\
&= \frac{2k^o}{\sqrt{\pi\alpha^o}}\frac{K_\varepsilon}{1+K_\varepsilon}\times\Bigg\{(\Delta T)h\sum_{n=1}^{N} h^{2(n-1)} \\
&\quad\times\left[\sqrt{t}\exp\left(-\left[\frac{(4n-0)R}{2\sqrt{\alpha^c t}}\right]^2\right)\right. \\
&\quad\left.-\frac{(4n-0)R}{2\sqrt{\alpha^c}}\sqrt{\pi}\,\mathrm{erfc}\frac{(4n-0)R}{2\sqrt{\alpha^c t}}\right] \\
&\quad+(-\Delta T)h\sum_{n=1}^{N} h^{2(n-1)} \\
&\quad\times\left[\sqrt{t}\exp\left(-\left[\frac{(4n-1)R}{2\sqrt{\alpha^c t}}\right]^2\right)\right. \\
&\quad\left.-\frac{(4n-1)R}{2\sqrt{\alpha^c}}\sqrt{\pi}\,\mathrm{erfc}\frac{(4n-1)R}{2\sqrt{\alpha^c t}}\right] \\
&\quad+(-\Delta T)\sum_{n=1}^{N} h^{2(n-1)} \\
&\quad\times\left[\sqrt{t}\exp\left(-\left[\frac{(4n-3)R}{2\sqrt{\alpha^c t}}\right]^2\right)\right. \\
&\quad\left.-\frac{(4n-3)R}{2\sqrt{\alpha^c}}\sqrt{\pi}\,\mathrm{erfc}\frac{(4n-3)R}{2\sqrt{\alpha^c t}}\right] \\
&\quad+(\Delta T)\sum_{n=1}^{N} h^{2(n-1)} \\
&\quad\times\left[\sqrt{t}\exp\left(-\left[\frac{(4n-4)R}{2\sqrt{\alpha^c t}}\right]^2\right)\right. \\
&\quad\left.-\frac{(4n-4)R}{2\sqrt{\alpha^c}}\sqrt{\pi}\,\mathrm{erfc}\frac{(4n-4)R}{2\sqrt{\alpha^c t}}\right]\Bigg\} \qquad (13)
\end{aligned}
$$

After a cycle of these three steps, one can get that the net heat flow through EC2|SO interface is

$$
Q_{\mathrm{SO}}^{\mathrm{net}} = -Q_{\mathrm{SO}}^{\mathrm{I}} - Q_{\mathrm{SO}}^{\mathrm{II}} + Q_{\mathrm{SO}}^{\mathrm{III}}. \qquad (14)
$$

4. Temperature Profile and Corresponding Heat Flow Through EC2|SO Interface

The directional heat transfer through the interface EC2|SO depends strongly on the interfacial temperature T_s[49,50] and the temperature profiles across the interface. The interfacial temperature T_s at interface EC2|SO is,

$$
T_s|_{\mathrm{EC2|SO}}(t) = \left.\frac{T_{\mathrm{EC2}}(t)\times K_\varepsilon + T_{\mathrm{SO}}(t)}{1+K_\varepsilon}\right|_{x=R}. \qquad (15)
$$

That is, T_s is determined by the surface temperature of two bodies at the surface and the relative thermal activity of bodies across the interface.

From Eq. (15), one can find that if SO/SI material is the same as ECM (i.e., $K_\varepsilon = 1$), T_s is simply the average of two surface temperatures and there will be a smooth temperature profile across the interface. If the $K_\varepsilon \to 0$, T_s will be very close to the temperature of the source surface ($x = R$), $T_{\mathrm{SO}}(t)|_{x=R}$. Therefore, $T_s(0^+)$ is close to the equilibrium temperature of SO, T. Similarly, if the $K_\varepsilon \to \infty, T_s$ will be very close to the temperature of the EC2 surface at $x = R$, $T_{\mathrm{EC2}}(t)|_{x=R}$.

For detailed study, numerical calculation was carried out using the mathematical model described in the Sec. 3 that was implemented in MATLAB. Thermal and physical properties of some commonly used materials are shown in Table 1. Following three special cases studied using the numerical method: (1) SO/SI material is the same as ECM (i.e., PMN-4.5PT), which results in $K_\varepsilon = 1$ (named as System-1); (2) BT as ECM and air as SO/SI, which results in $K_\varepsilon = 793.8 >> 1$ (named as System-2); (3) PMN-4.5PT is used as ECM and Cu is used as SO/SI material, which corresponds to an $K_\varepsilon = 0.0172 << 1$ (named as System-3). In all three systems, $R = 1$ mm was used. For the simulations, it was assumed that application/removal of an electric field on ECM (EC1 and EC2) results in a thermal change of $\Delta T_{\mathrm{EC}} = \pm 1^\circ$C, the corresponding change in heat energy is $\Delta Q = \rho R c_p \Delta T_{\mathrm{EC}}$ for unity cross-section of EC1/EC2 and the equilibrium temperature is 0°C. That is, in the calculation, 0°C is used as the equilibrium temperature, but the results can be simply used to any equilibrium temperature T. Therefore, T is used as the equilibrium temperature in the figures.

4.1. *Step-II and Step-III*

For system-1, as discussed in Sec. 2, the overall heat flow through the EC2|SO interface during Step-II and Step-III are not zero, but cancel each other as illustrated in Fig. 4 for the temperature profiles at different times. Clearly, the peak temperature location does not change with time. That is, when the temperature in all four bodies reaches their equilibrium temperature, the heat transferred through SI|EC1

Table 1. Properties of some EC and non-EC materials at room temperature.

Material	ρ (kg m^{-3})	c_p (JK^{-1}kg^{-1})	k (Wm^{-1}K^{-1})	α (m^{2}s^{-1}) (10^{-6})	Ref.
Air	1.16	1007	0.026	22.2	Ansys Library
PMN-4.5PT	8100	200	0.25	0.154	46
BT	6060	527	6	1.88	Ansys Library
Graphite	2250	709	24	15	Ansys Library
Aluminum	2689	951	237.5	92.9	Ansys Library
Silver	10,500	235	429	174	Ansys Library
Copper	8933	385	400	116	Ansys Library

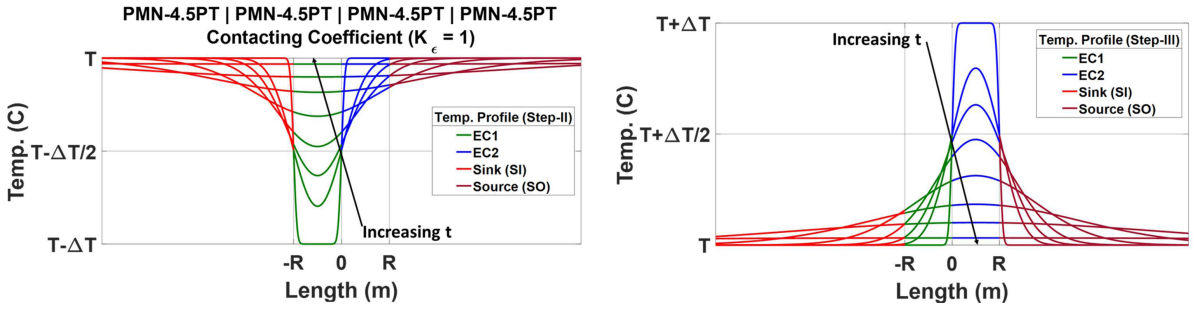

(a) (b)

Fig. 4. Temperature profiles of system-1 during: (a) Step-II, (b) Step-III, where $R = 1$ mm.

interface is exactly the same as the heat transferred through EC2|SO interface. If ΔQ is the heat absorbed by EC1 during Step-II and also the heat released by EC2 during Step-III, the net heat flows through EC2|SO is $-\Delta Q/2$ and $+\Delta Q/2$ during Step-II and Step-III, respectively.

For system-2, the temperature profiles during Step-II and Step-III at different times are shown in Fig. 5. Clearly, at the beginning the heat is mainly exchanged between EC1 and EC2, which results in a very small amount heat flows through EC2|SO and SI|EC1 interface, as illustrated in Fig. 6. In other words, the heat transferred between SI and EC1 and also between EC2 and SO mainly occurs after both EC1 and EC2 body reach the same temperature. Based on the results, it is concluded that the sum of the amount of net heat flows through EC2|SO interface during both Step-II and Step-III is zero as shown in Fig. 6.

For system-3, the temperature profiles at different times during Step-II and Step-III are plotted in Figs. 7(a) and 7(b), respectively. For Step-II, EC1 has to absorb an amount of heat (ΔQ) to reach the equilibrium temperature T with all other bodies. There is a point at which the temperature is the minimum.

The location of the minimum temperature shifts to right with time. At a certain time, the minimum temperature point is at $x = 0$. After this time, the heat flows from SO to EC2 with a higher rate than that from SI to EC1. Slowly, the minimum temperature point shifts to right further with time. At a certain time t_{II}, the minimum temperature point is at $x = R$.

After t_{II}, the heat flows back from EC2 to SO at EC2|SO interface, while at SI|EC1 interface, the heat is continuously flowing from SI to EC1. All these characteristics can be

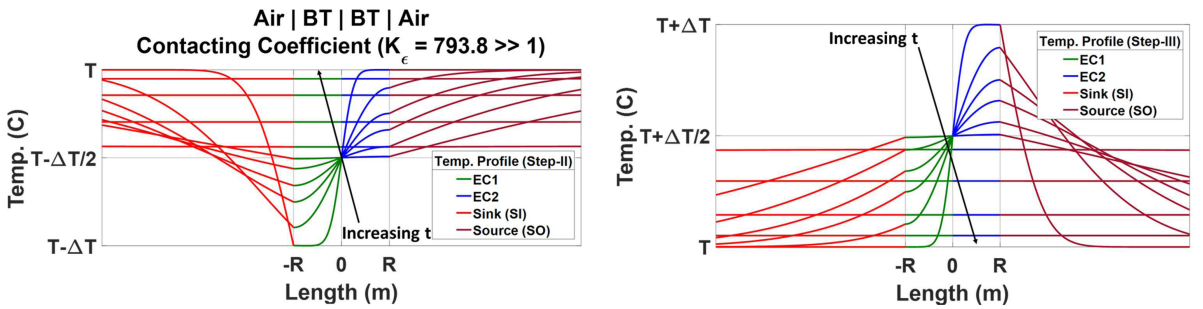

(a) (b)

Fig. 5. Temperature profiles of system-2 during: (a) Step-II, (b) Step-III, where $R = 1$ mm.

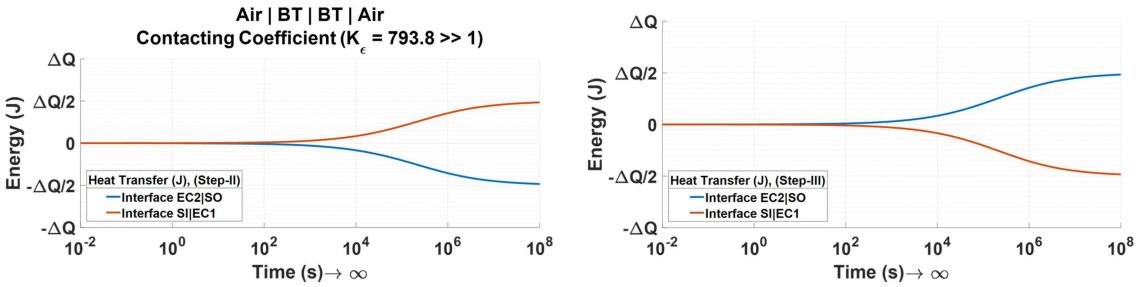

(a) (b)

Fig. 6. (Color online) Time dependence of heat energy transferred through SI|EC1 (blue) and EC2|SO (red) interface for system-2: (a) Step-II, (b) Step-III.

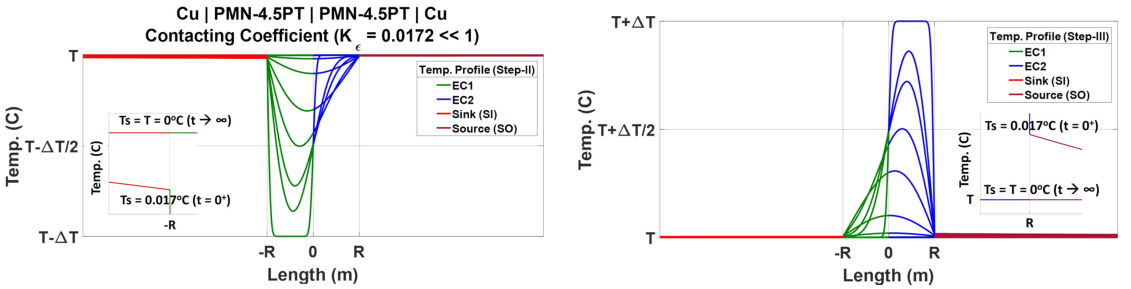

(a) (b)

Fig. 7. Temperature profiles of system-3 during: (a) Step-II, (b) Step-III, where $R = 1$ mm.

clearly seen from the time dependence of heat energy transferred through both interfaces as shown in Fig. 8.

As shown in Fig. 8(a), during Step-II, the heat transferred from SO to EC2 is continuously increasing, but the heat transferred from SI to EC1 increases initially and, then, decreases with time. Eventually, all four bodies reach their equilibrium temperature T and the heat transferred from SI to EC1 reaches the same value as the heat transferred from EC2 to SO. That is, for a complete Step-II, the net heat transferred from SO to EC2 is exactly $\Delta Q/2$. Similarly, the heat transferred from SI to EC1 is also $\Delta Q/2$.

The heat transformation during Step-III is exactly the same as Step-II except the direction of heat flow. Again, eventually, all four bodies reach their equilibrium temperature T and the net heat transferred from EC2 to SO is exactly the same as the heat transferred from EC1 to SI (i.e., $\Delta Q/2$) as shown in Fig. 8(b).

Based on the results obtained from Step-II and Step-III, it is concluded that the sum of the amount of heat flows through EC2|SO interface during both Step-II and Step-III is zero.

4.2. *Step-I*

The temperature profile for system-1 at different times is shown in Fig. 9(a). Clearly, the temperature is symmetrical around $x = 0$. There are two characteristic points: one at which the temperature is the maximum, the other at which the temperature is minimum. The location of these two points, which shifts away from $x = 0$ with time, has the same distance from $x = 0$.

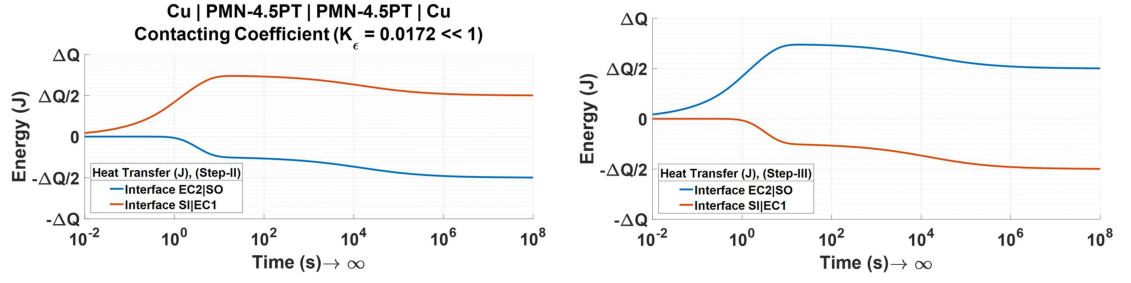

(a) (b)

Fig. 8. (Color online) Time dependence of heat energy transferred through SI|EC1 (blue) and EC2|SO (red) interface for system-3: (a) Step-II, (b) Step-III.

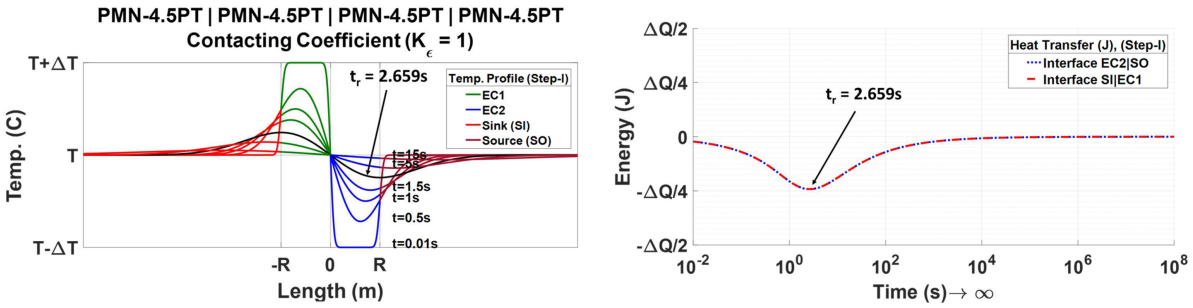

(a) (b)

Fig. 9. Step-I of system-1: (a) Temperature profiles at different times, Arrowhead shows the curve at the time $t_r(\partial T_s(t_r)/\partial x|_{x=R} = 0)$, (b) Time dependence of heat energy transferred through the interfaces EC2|SO and SI|EC1.

From the results shown in Fig. 9(a), one can find that at the beginning, temperature gradient at the interface ($x = R$) is positive, meaning there is a heat flow from the source (SO) to EC2 (also from EC1 to SI). As time goes on, the temperature gradient at the interface decreases, meaning heat flow rate decreases.

At a certain time (t_r), the temperature gradient at the interface reaches zero. After time t_r, the heat flows back from EC2 to SO, which is illustrated in Fig. 9(b). In other words, after the time t_r, the process reduces the heat to be removed from the source.

All these indicate that t_r is a critical time for the system. The value of t_r for different systems that use different ECMs and SO/SI materials is presented in Table 2. The value of t_r is dependent on the thermal conductivity of the materials. For example, as shown in Table 2, the t_r is 2.6585 s and 0.2184 s for a system made of PMN-4.5PT and BT, respectively.

For system-2, the temperature profile is shown in Fig. 10(a), and corresponding heat exchange between SO and EC2 is illustrated in Fig. 10(b). Again, it is concluded that for a complete Step-1, there is no heat transferred between SO and SI.

The temperature profile for system-3 is shown in Fig. 11(a). Similar to system-1, the temperature profile is symmetrical around $x = 0$ with a maximum and a minimum. The distance from the location of temperature maximum to $x = 0$ is the same as that of temperature minimum to $x = 0$. The location of temperature maximum and minimum shifts away from $x = 0$ with time.

At time t_r, the location of the temperature maximum is at $x = -R$, while the location of the temperature minimum is at $x = R$. After time t_r, the location of the temperature minimum is at $x > R$, while the location of the temperature maximum is at $x < -R$. In other words, the heat is initially transferred from SO to EC2 and EC1 to SI. However, after time t_r, the heat flows back from EC2 to SO and SI to EC1, as illustrated in Fig. 11(b). If time is long enough, it is found that the overall heat exchange between SO and EC2 is zero, as well as between SI and EC1. Therefore, for a completed Step-I, there is no heat transferred from SO to SI.

Table 2. Contacting coefficient (K_ε), interface temperature (T_s) at EC2|SO interface at $t = 0$ and t_r, timet_r and $Q(t_r)$ for systems using BT and PMN-4.5PT as ECM and different materials as SO and SI. ($\delta = 10^{-5}$).

EC1/EC2	SI/SO	$\rho^o c_p^o$ (10^6)	K_ε	$T_s = \Delta T(\frac{K_\varepsilon}{1+K_\varepsilon})$ at $t = 0^+$	t_r (s)	$T_s(t_r)$ (°C)	Q (t_r) (J)	System	$Q_r(\%) = \frac{Q(t_r)}{\Delta Q} \times 100$
BT $\Delta T = 1.0$°C	**Art**	0.00117	**793.8**	**−0.999**	**0.1932**	**−0.530**	**1.86**	**System-2**	**0.06**
$\Delta Q = 3194$ J	PMN-4.5PT	1.620	6.878	−0.908	0.1979	−0.400	188.3		6.0
$\rho^c c_p^c = 3.19 \times 10^6$	BT	3.190	1	−1/2	0.2184	−0.076	749.8		23.8
	Gr	0.056	0.708	−0.412	0.2257	−0.150	881.0		27.6
	Al	2.557	0.178	−0.15	0.2683	−0.065	1294		40.5
	Ag	2.468	0.135	−0.12	0.2791	−0.051	1346.5		42.2
	Cu	3.439	0.118	−0.11	0.2846	−0.044	1368.1		42.8
PMN−4.5PT $\Delta T = 1.0$°C	Air	0.00117	115.4	−0.990	2.3545	−0.520	6.596		0.41
$\Delta Q = 1620$ J	**PMN-4.5PT**	1.620	**1**	**−1/2**	**2.6585**	**−0.244**	**389.1**	**System-1**	**24.0**
$\rho^c c_p^c = 1.62 \times 10^6$	BT	3.190	0.145	−0.126	3.3601	−0.0110	691.4		42.6
	Gr	0.056	0.103	−0.092	3.527	−0.0389	719.9		44.4
	Al	2.557	0.026	−0.020	4.3121	−0.0094	779.3		48.1
	Ag	2.468	0.020	−0.025	4.4812	−0.0070	784.7		48.4
	Cu	3.439	**0.017**	**−0.017**	**4.5637**	**−0.0061**	**786.9**	**System-3**	**48.6**

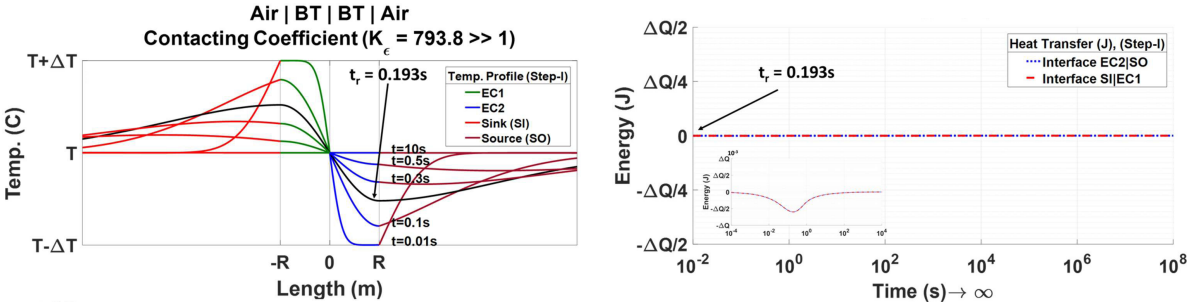

(a) (b)

Fig. 10. Step-I of system-2: (a) Temperature profile at different times, (b) Time dependence of heat energy transferred through the interfaces EC2|SO and SI|EC1.

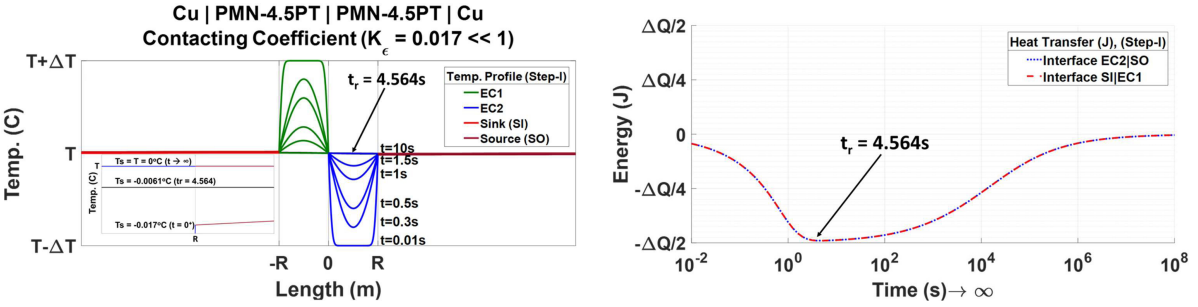

(a) (b)

Fig. 11. Step-I of system-3 with $R = 1\,\text{mm}$, $\Delta T = 1^\circ\text{C}$: (a) Temperature profile, arrowhead shows the curve at the time t_r; (b) Time dependence of heat energy transferred through the interfaces EC2|SO and SI|EC1.

In a brief summary, for all three systems, it is found that when the time is long enough, all four bodies reach their equilibrium temperature T, which corresponds to an overall heat amount transferred through the interface is zero for Step-I.

4.3. *Summary of an ideal three-step process*

Based on the results obtained above, for the three-step process described in Fig. 2, if each step reaches its final equilibrium state (i.e., each step is operated with a long enough time), there is no net heat flow through the EC2|SO and SI|EC1 interfaces. In other words, after a complete cycle, no heat is transferred from SO to SI.

5. Operation to Achieve Net Heat Tranferred from SO to SI for One Cycle for $K_\varepsilon \ll 1$

As discussed above, the heat transferred between EC2 and SO during Step-II and Step-III cancels each other. Therefore, the net heat transformation between SO and SI for the system and process described in Sec. 2 is dependent on Step-I. However, as demonstrated above, for Step-I, initially heat flows from SO to EC2, but after time t_r, the heat flows back from EC2 to SO. Therefore, if Step-II can start at the time t_r of Step-I a nonzero net heat can be transferred from SO to SI. However, when K_ε is big, the temperature in the ECM at t_r is significantly different to the equilibrium temperature. Fortunately, when K_ε is very small, the T_s at t_r is very close to the equilibrium temperature T and at the same time a higher $Q(t_r)$ is obtained as shown in Table 2. From the data shown in Table 2, one can find that the smaller the K_ε, the higher the $Q(t_r)$ is and the smaller the T_s is. Therefore, to build a cooling pump using the design reported here, a smaller K_ε is better.

For system-3 ($K_\varepsilon = 0.0172$), at time t_r, the temperature at the surface of EC2 ($x = R$) is the lowest temperature in EC2, which is only 0.0061°C different from the equilibrium temperature T or 0.61% of the temperature change ($\Delta T = 1^\circ$C) induced in ECM by the ECE. Considering the temperature in EC2 is not uniform, one side is always the same as the equilibrium temperature and the other side only 0.0061°C different with the equilibrium temperature, the average temperature in EC2 is only about 0.003°C or 0.3% of ΔT. Therefore, when Step-II starts at the time t_r of Step-I, the results obtained in Section IV (A) for Step-II and Step-III are still valid. Therefore, after a three-step process cycle with Step-1 completed at t_r, a nonzero amount of heat is transferred from SO to EC2, which is also the heat transferred from EC1 to SI. It has to be mentioned that the initial temperature (i.e., equilibrium temperature) of both SO and SI are the same. In other words, for SO and SI with the same temperature, amount of heat, $Q(t_r)$, is transferred from SO to SI by one cycle. From Table 2, it is found that the overall heat

Table 3. Step-I of system-3 when it is operated with different ΔT. ($\delta = 10^{-5}$).

$\Delta T(^\circ)$	ΔQ (J) $R = 1$ mm	$T_s(t = 0^+)$ (°C)	t_r (s)	$T_s(t_r)$ (°C)	$\frac{T_s(t_r)}{\Delta T}$	$Q(t_r)$	$Q_r = \frac{Q(t_r)}{\Delta Q}$
1	1620	−0.017	4.564	−0.0061	−0.0061	786.9	48.6%
2	3240	−0.034	4.564	−0.0121	−0.0061	1573.8	48.6%
5	8100	−0.085	4.564	−0.0304	−0.0061	3935	48.6%
10	16,200	−0.170	4.564	−0.0607	−0.0061	7869	48.6%

Table 4. System-3 is modified to use the ECM layers with different R.

R (mm)	t_r (s)	Ts (t_r)	$Q(t_r)$ (J)	ΔQ (J)	$Q(t_r)/\Delta Q$ (%)	$Q(t_r)/t_r$
0.1	0.0457	−0.0061	72.5	162	44.7	1586.4
0.3	0.4108	−0.0061	231.2	486	47.6	562.8
0.5	1.1410	−0.0061	390	810	48.1	341.8
0.7	2.2363	−0.0061	548.7	1134	48.4	245.4
1.0	**4.5637**	**−0.0061**	**786.9**	**1620**	**48.6**	**172.4**
1.5	10.2683	−0.0061	1183.7	2430	48.7	115.3
2.0	18.2548	−0.0061	1580.6	3240	48.8	86.6
3.0	41.0740	−0.0061	2374.4	4860	48.9	57.8
4.0	73.0189	−0.0061	3168.2	6480	48.9	43.4
5.0	114.10	−0.0061	3862.0	8100	48.9	33.84

transferred from SO to EC2, which is also the heat transferred from EC1 to SI, is about 49% of ΔQ — the thermal energy induced in the EC2 by the ECE.

For system-3, when different ΔT is used to operate it (i.e., different electric field is used), the results are shown in Table 3. One can find that all the values of t_r, $T_s(t_r)/\Delta T$ and $Q(t_r)/\Delta Q$ do not change. In other words, the calculated results can be easily modified to the system operated under different electric field (i.e., different ΔT).

When system-3 is modified by using EC1/EC2 with different thicknesses, the results are shown in Table 4. From the results in Table 4, one can find that although the t_r increases with the R, the $T_s(t_r)$ does not change with R. That is, the thickness does not affect the $T_s(t_r)$ which is only about 0.3% of ΔT.

Based on the results shown in Tables 3 and 4, it is concluded that $T_s(t_r)/\Delta T$ is independent on the R and ΔT. In other words, T_s at t_r during Step-1 is only 0.3% of ΔT. Therefore, the operation introduced here by starting Step-II at time t_r of Step-I works for all the systems as long as K_ε is very small. To achieve a larger amount of heat energy transferred from SO to SI during one cycle (i.e., a higher $Q(t_r)$), a smaller contacting coefficient (K_ε) is certainly required. Based on the definition in Sec. 3,

$$K_\varepsilon = \sqrt{\frac{k^c \rho^c c_p^c}{k^o \rho^o c_p^o}}, \tag{16}$$

where $\rho^c c_p^c$ and $\rho^o c_p^o$ are the volumetric specific heat capacity of ECM and SO/SI material, respectively. Therefore, to achieve a smaller contacting coefficient, SO/SI with a higher thermal conductivity and a higher volumetric heat capacity would be favorable.

To increase the power transformation rate, a smaller t_r is desired. From Eq. (11), one can find that the time dependence of the heat transfer through EC2|SO interface is actually dependent on α^c and $h = (1 - K_\varepsilon)/(1 + K_\varepsilon)$.

6. Conclusion and Comments

A new design of heat pump using ECE is introduced by using two layers of ECM. The electric field applied on both ECM layers is independently controlled with a sequence (i.e., process) that includes three steps and can be repeated continuously. Among three steps, Step-I is used to transfer heat from SO to SI, while Step-II and Step-III are used to restore the initial condition for Step-I so that the process can be repeated continuously. The time dependences of both the temperature profile in all four bodies and heat transformation through the interface were calculated using the newly introduced analytical solutions. It is concluded that the heat transformation during Step-II and Step-III cancels each other. Therefore, the amount of heat transferred from SO to SI during Step-I is the net heat transferred for one cycle. During Step-I, one layer of ECM increases, and the other layer of ECM decreases its temperature simultaneously using ECE. There is a critical time, t_r, at which the maximum and minimum point of the temperature profile are at SI|EC1 and EC2|SO interfaces. Step-II has to start at time t_r of Step-I. To achieve a larger amount of heat transferred from SO to SI, it is concluded that: (1) the SO and SI should have a much higher thermal conductivity than the ECM; (2) the SO/SI material with a higher volumetric heat capacity is also favorable.

By using PMN-4.5PT as ECM, and Cu as SI/SO materials, it is demonstrated that during Step-I the amount of heat transferred

from SO to SI is about 49% of the heat generated in one ECM layer due to the ECE, which is independent of both the thickness of ECM and the ΔT — temperature change in ECM due to the ECE. However, the time t_r increases with increasing thickness of ECM layer, but does not change with the ΔT. That is, the ECE heat pump introduced in here can transfer heat from SO to SI for both SO and SI with the same equilibrium temperature. It has to be mentioned that in this design, neither moving part nor heat switch was used, so this concept not only offers a reliable thermal contact, but also a directional heat flow in complete silent operation has been achieved eliminating the usage of any additional mechanism and making it feasible to be exploited in microscale applications.

Application Remark: Given that unidirectional heat flow was achieved without any moving parts with the ECE heat pump unit concept presented in this paper, future work might focus on staggering and cascading multiple EC heat pump units. Series and parallel configurations could produce larger temperature lifts and higher heat transfer rates more typical of heat pump systems for applications from electronic cooling to building and transportation HVAC systems.

Acknowledgments

F.N. appreciates the financial support from the U.S. Department of State, Bureau of Educational and Cultural Affairs (ECA) and the United States Agency for International Development (USAID), as well as the administrative support from the United States Educational Foundation in Pakistan (USEFP) and the Institute of International Education (IIE), throughout his research as a Ph.D. candidate under the Fulbright Foreign Student Program.

Data Availability

The data that support the findings of this study are available from the corresponding author and first author upon reasonable request.

References

[1]James R. Sand, Steven K. Fischer and Van D. Baxter, *Energy and Global Warming Impacts of HFC Refrigerants and Emerging Technologies* (1997).
[2]UN, *Kyoto Protocol to the United Nations Framework Convension on Climate Change* (1998).
[3]S. Qian *et al.*, Not-in-kind cooling technologies: A quantitative comparison of refrigerants and system performance. *Int. J. Refrig.* **62**, 177 (2016).
[4]A. Kitanovski *et al.*, *Magnetocaloric Energy Conversion: From Theory to Applications* (Springer, 2015).
[5]M. Ožbolt, A. Kitanovski, J. Tušek and A. Poredoš, Electrocaloric vs. magnetocaloric energy conversion, *Int. J. Refrig.* **37**, 16 (2014).
[6]B. Rožič *et al.*, Influence of the critical point on the electrocaloric response of relaxor ferroelectrics, *J. Appl. Phys.* **110**, 064118 (2011).
[7]U. Plaznik *et al.*, Bulk relaxor ferroelectric ceramics as a working body for an electrocaloric cooling device, *Appl. Phys. Lett.* **106**, 043903 (2015).
[8]Q. Zhang and T. Correia, *Electrocaloric Materials: New Generation of Coolers* (Springer, 2014).
[9]Q. Zhang and T. Correia, Electrocaloric effect: An introduction, in *Electrocaloric Matrials: New Generation of Coolers* (Heidelberg, Springer, 2014), pp. 1–14.
[10]Y. V. Sinyavsky and V. M. Brodyansky, Experimental testing of electrocaloric cooling with transparent ferroelectric ceramic as a working body, *Ferroelectrics* **131**, 321 (1992).
[11]M. Valant, Electrocaloric materials for future solid-state refrigeration technologies, *Prog. Mater. Sci.* **57**, 980–1009 (1009).
[12]A. S. Mischenko, Q. Zhang, J. F. Scott, R. W. Whatmore and N. D. Mathur, Giant electrocaloric effect in thin-film $PbZr_{0.95}Ti_{0.05}O_3$, *Science* **311**, 1270 (2006).
[13]B. Neese *et al.*, Large electrocaloric effect in ferroelectric polymers near room temperature, *Science* **321**, 821 (2008).
[14]X. S. Qian *et al.*, Giant electrocaloric response over a broad temperature range in modified $BaTiO_3$ ceramics, *Adv. Funct. Mater.* **24**, 1300 (2014).
[15]Y. Liu and G. Zheng, Anelastic analyses on the relaxation of antiferroelectric states in 0.94Bi0.5Na0.5TiO3-0.06BaTiO3 solid solutions under electric fields, *J. Electroceram.* **34**, 38 (2015).
[16]X.-D. Jian *et al.*, Direct measurement of large electrocaloric effect in $Ba(Zr_x\ Ti_{1-x})O_3$ ceramics, *ACS Appl. Mater. Interfaces* **10**, 4801 (2018).
[17]D. Guo *et al.*, The giant electrocaloric effect and high effective cooling power near room temperature for $BaTiO_3$ thick film, *J. Appl. Phys.* **110**, 094103 (2011).
[18]A. S. Mischenko, Q. Zhang, R. W. Whatmore, J. F. Scott and N. D. Mathur, Giant electrocaloric effect in the thin film relaxor ferroelectric 0.9 Pb Mg1/3Nb2/3O3-0.1 PbTiO3 near room temperature, *Appl. Phys. Lett.* **89**, 1 (2006).
[19]N. Novak, Z. Kutnjak and R. Pirc, High-resolution electrocaloric and heat capacity measurements in barium titanate, *Europhys. Lett.* **103**, 47001 (2013).
[20]Y. Zhao, X. Hao and Q. Zhang, A giant electrocaloric effect of a Pb0.97La0.02(Zr0.75Sn0.18Ti0.07)O3 antiferroelectric thick film at room temperature, *J. Mater. Chem. C* **3**, 1694 (2015).
[21]B. Peng, H. Fan and Q. Zhang, A giant electrocaloric effect in nanoscale antiferroelectric and ferroelectric phases coexisting in a relaxor Pb0.8Ba 0.2ZrO3 thin film at room temperature, *Adv. Funct. Mater.* **23**, 2987 (2013).
[22]A. Kumar, A. Thakre, D. Y. Jeong and J. Ryu, Prospects and challenges of the electrocaloric phenomenon in ferroelectric ceramics, *J. Mater. Chem. C* **7**, 6836 (2019).
[23]Y. Liu, J. F. Scott and B. Dkhil, Direct and indirect measurements on electrocaloric effect: Recent developments and perspectives, *Appl. Phys. Rev.* **3**, 031102 (2016).
[24]J. Shi *et al.*, Electrocaloric cooling materials and devices for zero-global-warming-potential, high-efficiency refrigeration, *Joule* **3**, 1200 (2019).
[25]P. Blumenthal and A. Raatz, Classification of electrocaloric cooling device types, *Europhys. Lett.* **115**, 17004 (2016).
[26]R. Chukka, S. Shannigrahi and L. Chen, Investigations of cooling efficiencies in solid-state electrocaloric device, *Integ. Ferroelectrics* **133**, 3 (2012).
[27]M. Ožbolt, A. Kitanovski, J. Tušek and A. Poredoš, Electrocaloric refrigeration: Thermodynamics, state of the art and future perspectives, *Int. J. Refrig.* **40**, 174 (2014).

[28]P. Blumenthal, C. Molin, S. Gebhardt and A. Raatz, Active electrocaloric demonstrator for direct comparison of PMN-PT bulk and multilayer samples, *Ferroelectrics* **497**, 1 (2016).
[29]D. Guo *et al.*, Design and modeling of a fluid-based micro-scale electrocaloric refrigeration system, *Int. J. Heat Mass Transf.* **72**, 559 (2014).
[30]A. Kitanovski, U. Plaznik, U. Tomc and A. Poredoš, Present and future caloric refrigeration and heat-pump technologies, *Int. J. Refrig.* **57**, 288 (2015).
[31]X. Li, H. Gu, X. Qian and Q. Zhang, Compact cooling devices based on giant electrocaloric effect dielectrics, *13th InterSociety Conf. Thermal and Thermomechanical Phenomena in Electronic Systems* (IEEE, 2012), pp. 934–937. doi: 10.1109/ITHERM.2012.6231525.
[32]H. Gu *et al.*, A chip scale electrocaloric effect based cooling device, *Appl. Phys. Lett.* **102**, 122904 (2013).
[33]H. Gu, X. S. Qian, H. J. Ye and Q. M. Zhang, An electrocaloric refrigerator without external regenerator, *Appl. Phys. Lett.* **105**, 162905-1-162905–4 (2014).
[34]T. Zhang, X. S. Qian, H. Gu, Y. Hou and Q. M. Zhang, An electrocaloric refrigerator with direct solid to solid regeneration, *Appl. Phys. Lett.* **110**, 243503 (2017).
[35]Y. S. Ju, Solid-state refrigeration based on the electrocaloric effect for electronics cooling, *J. Electronic Packaging* **132**, 041004 (2010).
[36]R. Ma *et al.*, Highly efficient electrocaloric cooling with electrostatic actuation, *Science* **357**, 1130 (2017).
[37]A. Bradesko *et al.*, Coupling of the electrocaloric and electromechanical effects for solid-state refrigeration, *Appl. Phys. Lett.* **109**, 143508 (2016).
[38]Y. Jia and Y. Sungtaek Ju, A solid-state refrigerator based on the electrocaloric effect, *Appl. Phys. Lett.* **100**, 242901 (2012).
[39]R. I. Epstein and K. J. Malloy, Electrocaloric devices based on thin-film heat switches, *J. Appl. Phys.* **106**, 064509 (2009).
[40]D. Feng, S. Yao, T. Zhang and Q. Zhang, Modeling of smart heat pump using thermoelectric and electrocaloric materials, *J. Electronic Packaging* **138**, 041004 (2016).
[41]S. J. Smullin, Y. Wang and D. E. Schwartz, System optimization of a heat-switch-based electrocaloric heat pump, *Appl. Phys. Lett.* **107**, 093903-1-093903–4 (2015).
[42]Y. D. Wang *et al.*, A heat-switch-based electrocaloric cooler, *Appl. Phys. Lett.* **107**, 134103 (2015).
[43]S. F. Karmanenko, O. V. Pakhomov, A. M. Prudan, A. S. Starkov and A. Eskov, Layered ceramic structure based on the electrocaloric elements working as a solid state cooling line, *J. Eur. Ceram. Soc.* **27**, 3109 (2007).
[44]A. V. Es'kov, S. F. Karmanenko, O. V. Pakhomov and A. S. Starkov, Simulation of a solid-state cooler with electrocaloric elements, *Phys. Solid State* **51**, 1574 (2009).
[45]O. V. Pakhomov, S. F. Karmanenko, A. A. Semenov and A. S. Starkov, Thermodynamic estimation of cooling efficiency using an electrocaloric solid state line, *Tech. Phys.* **55**, 1155 (2010).
[46]A. Khodayari and S. Mohammadi, Solid-state cooling line based on the electrocaloric effect, *IEEE Trans. Ultrasonics Ferroelectrics Freq. Control* **58**, 503 (2011).
[47]Y. Bai, G. P. Zheng and S. Q. Shi, Kinetic electrocaloric effect and giant net cooling of lead-free ferroelectric refrigerants, *J. Appl. Phys.* **108**, 104102 (2010).
[48]F. Najmi, W. Shen, L. Cremaschi and Z. Cheng, Electrocaloric devices part I: Analytical solution of one-dimensional transient heat conduction in a multilayer electrocaloric system, *J. Adv. Dielectrics* **10**, 2050028 (2020).
[49]A. Luikov, *Analytical Heat Diffusion Theroy* (Academic Press, 1968).
[50]R. C. Xin and W. Q. Tao, Analytical solution for transient heat conduction in two semi-infinite bodies in contact, *ASME* **116**, 224 (1994).

Supplementary Information (SI)

S1. Temperature Profiles

S1.1. *Temperature profile of EC2 body*

$$
\begin{aligned}
&T_{\mathrm{EC2}}(x,t)-T_{\mathrm{EC2},i}\\
&\quad=-\frac{(T_{\mathrm{EC1},i}-T_{\mathrm{EC2},i})h^2}{2}\sum_{n=1}^{\infty}h^{2(n-1)}\\
&\qquad\times\operatorname{erfc}\frac{(4n-0)R-x}{2\sqrt{\alpha^c t}}+\frac{h}{1+K_\varepsilon}\sum_{n=1}^{\infty}h^{2(n-1)}\\
&\qquad\times\left[(T_{\mathrm{EC1},i}-T_{\mathrm{SI},i})\operatorname{erfc}\frac{(4n-1)R-x}{2\sqrt{\alpha^c t}}\right.\\
&\qquad\left.+\ (T_{\mathrm{EC2},i}-T_{\mathrm{SO},i})\operatorname{erfc}\frac{(4n-1)R+x}{2\sqrt{\alpha^c t}}\right]\\
&\qquad-\frac{h}{2}\sum_{n=1}^{\infty}h^{2(n-1)}\big[(T_{\mathrm{EC1},i}-T_{\mathrm{EC2},i})\\
&\qquad\times\operatorname{erfc}\frac{(4n-2)R-x}{2\sqrt{\alpha^c t}}-(T_{\mathrm{EC1},i}-T_{\mathrm{EC2},i})\\
&\qquad\times\operatorname{erfc}\frac{(4n-2)R+x}{2\sqrt{\alpha^c t}}\Big]-\tfrac{1}{1+K_\varepsilon}\sum_{n=1}^{\infty}h^{2(n-1)}\\
&\qquad\times\left[(T_{\mathrm{EC2},i}-T_{\mathrm{SO},i})\operatorname{erfc}\frac{(4n-3)R-x}{2\sqrt{\alpha^c t}}\right.\\
&\qquad\left.+(T_{\mathrm{EC1},i}-T_{\mathrm{SI},i})\operatorname{erfc}\frac{(4n-3)R+x}{2\sqrt{\alpha^c t}}\right]\\
&\qquad+\frac{(T_{\mathrm{EC1},i}-T_{\mathrm{EC2},i})}{2}\sum_{n=1}^{\infty}h^{2(n-1)}\\
&\qquad\times\operatorname{erfc}\frac{(4n-4)R+x}{2\sqrt{\alpha^c t}}
\end{aligned}
\tag{S.1}
$$

S2. Temperature Profile of SO Body

$$
\begin{aligned}
&T_{\mathrm{SO}}(x,t)-T_{\mathrm{SO},i}\\
&\quad=\frac{K_\varepsilon}{1+K_\varepsilon}\left\{(T_{\mathrm{EC2},i}-T_{\mathrm{SO},i})h\sum_{n=1}^{\infty}h^{2(n-1)}\right.\\
&\qquad\left.\times\operatorname{erfc}\frac{x-R+(4n-0)K_\alpha^{-1/2}R}{2\sqrt{\alpha^o t}}+(T_{\mathrm{EC1},i}-T_{\mathrm{EC2},i})\right.
\end{aligned}
$$

$$
\begin{aligned}
&\times h\sum_{n=1}^{\infty} h^{2(n-1)}\operatorname{erfc}\frac{x-R+(4n-1)K_\alpha^{-1/2}R}{2\sqrt{\alpha^o t}}\\
&-\frac{2(T_{\mathrm{EC1},i}-T_{\mathrm{SI},i})}{1+K_\varepsilon}\sum_{n=1}^{\infty} h^{2(n-1)}\\
&\times \operatorname{erfc}\frac{x-R+(4n-2)K_\alpha^{-1/2}R}{2\sqrt{\alpha^o t}}\\
&+(T_{\mathrm{EC1},i}-T_{\mathrm{EC2},i})\sum_{n=1}^{\infty} h^{2(n-1)}\\
&\times \operatorname{erfc}\frac{x-R+(4n-3)K_\alpha^{-1/2}R}{2\sqrt{\alpha^o t}}\\
&+(T_{\mathrm{EC2},i}-T_{\mathrm{SO},i})\sum_{n=1}^{\infty} h^{2(n-1)}\\
&\times \operatorname{erfc}\frac{x-R+(4n-4)K_\alpha^{-1/2}R}{2\sqrt{\alpha^o t}}\Bigg\}
\end{aligned}
\tag{S.2}
$$

S3. Heat Flux Through the Interfaces

S3.1. *Heat fluxes through interface SI|EC1*

$$
\begin{aligned}
&q_{\mathrm{SI|EC1}}(t)\\
&\quad=-k^o\frac{\partial T_{\mathrm{SI}}(x,t)}{\partial x}\bigg|_{x=-R}\\
&\quad=-\frac{k^o}{\sqrt{\pi\alpha^o t}}\frac{K_\varepsilon}{1+K_\varepsilon}\\
&\qquad\times\Bigg\{(T_{\mathrm{EC1},i}-T_{\mathrm{SI},i})h\sum_{n=1}^{N} h^{2(n-1)}\\
&\qquad\times\exp\left(-\left[\frac{(4n-0)R}{2\sqrt{\alpha^c t}}\right]^2\right)\\
&\qquad-(T_{\mathrm{EC1},i}-T_{\mathrm{EC2},i})h\sum_{n=1}^{N} h^{2(n-1)}\\
&\qquad\times\exp\left(-\left[\frac{(4n-1)R}{2\sqrt{\alpha^c t}}\right]^2\right)\\
&\qquad-\frac{2(T_{\mathrm{EC2},i}-T_{\mathrm{SO},i})}{(1+K_\varepsilon)}\sum_{n=1}^{N} h^{2(n-1)}\\
&\qquad\times\exp\left(-\left[\frac{(4n-2)R}{2\sqrt{\alpha^c t}}\right]^2\right)\\
&\qquad-(T_{\mathrm{EC1},i}-T_{\mathrm{EC2},i})\sum_{n=1}^{N} h^{2(n-1)}\\
&\qquad\times\exp\left(-\left[\frac{(4n-3)R}{2\sqrt{\alpha^c t}}\right]^2\right)\\
&\qquad+(T_{\mathrm{EC1},i}-T_{\mathrm{SI},i})\sum_{n=1}^{N} h^{2(n-1)}\\
&\qquad\times\exp\left(-\left[\frac{(4n-4)R}{2\sqrt{\alpha^c t}}\right]^2\right)\Bigg\}
\end{aligned}
\tag{S.3}
$$

S3.2. *Heat flux through interface EC2|SO*

$$
\begin{aligned}
&q_{\mathrm{EC2|SO}}(t)\\
&\quad=-k^o\frac{\partial T_{\mathrm{SO}}(x,t)}{\partial x}\bigg|_{x=R}\\
&\quad=\frac{k^o}{\sqrt{\pi\alpha^o t}}\frac{K_\varepsilon}{1+K_\varepsilon}\times\big\{(T_{\mathrm{EC2},i}-T_{\mathrm{SO},i})\\
&\qquad\times h\sum_{n=1}^{N} h^{2(n-1)}\exp\left(-\left[\frac{(4n-0)R}{2\sqrt{\alpha^c t}}\right]^2\right)\\
&\qquad+(T_{\mathrm{EC1},i}-T_{\mathrm{EC2},i})h\sum_{n=1}^{N} h^{2(n-1)}\\
&\qquad\times\exp\left(-\left[\frac{(4n-1)R}{2\sqrt{\alpha^c t}}\right]^2\right)-\frac{2(T_{\mathrm{EC1},i}-T_{\mathrm{SI},i})}{(1+K_\varepsilon)}\\
&\qquad\times\sum_{n=1}^{N} h^{2(n-1)}\exp\left(-\left[\frac{(4n-2)R}{2\sqrt{\alpha^c t}}\right]^2\right)\\
&\qquad+(T_{\mathrm{EC1},i}-T_{\mathrm{EC2},i})\sum_{n=1}^{N} h^{2(n-1)}\\
&\qquad\times\exp\left(-\left[\frac{(4n-3)R}{2\sqrt{\alpha^c t}}\right]^2\right)+(T_{\mathrm{EC2},i}-T_{\mathrm{SO},i})\\
&\qquad\times\sum_{n=1}^{N} h^{2(n-1)}\exp\left(-\left[\frac{(4n-4)R}{2\sqrt{\alpha^c t}}\right]^2\right)\Bigg\}
\end{aligned}
\tag{S.4}
$$

S4. Energy Transfer through SI|EC1

The total energy transfer through the interface may be determined as follows.

$$
\begin{aligned}
&Q_{\mathrm{SI|EC1}}=\int_0^t q_{\mathrm{SI|EC1}}(t)dt\\
&Q_{\mathrm{SI|EC1}}=-\frac{2k^o}{\sqrt{\pi\alpha^o}}\frac{K_\varepsilon}{1+K_\varepsilon}\\
&\qquad\times\Bigg\{(T_{\mathrm{EC1},i}-T_{\mathrm{SI},i})h\sum_{n=1}^{N} h^{2(n-1)}\\
&\qquad\times\left[\sqrt{t}\exp\left(-\left[\frac{(4n-0)R}{2\sqrt{\alpha^c t}}\right]^2\right)\right.\\
&\qquad\left.-\frac{(4n-0)R}{2\sqrt{\alpha^c}}\sqrt{\pi}\operatorname{erfc}\frac{(4n-0)R}{2\sqrt{\alpha^c t}}\right]\\
&\qquad-(T_{\mathrm{EC1},i}-T_{\mathrm{EC2},i})h\sum_{n=1}^{N} h^{2(n-1)}\\
&\qquad\times\left[\sqrt{t}\exp\left(-\left[\frac{(4n-1)R}{2\sqrt{\alpha^c t}}\right]^2\right)\right.\\
&\qquad\left.-\frac{(4n-1)R}{2\sqrt{\alpha^c}}\sqrt{\pi}\operatorname{erfc}\frac{(4n-1)R}{2\sqrt{\alpha^c t}}\right]\\
&\qquad-\frac{2(T_{\mathrm{EC2},i}-T_{\mathrm{SO},i})}{(1+K_\varepsilon)}\sum_{n=1}^{N} h^{2(n-1)}
\end{aligned}
$$

$$\times\left[\sqrt{t}\exp\left(-\left[\frac{(4n-2)R}{2\sqrt{\alpha^c t}}\right]^2\right)\right.$$
$$\left.-\frac{(4n-2)R}{2\sqrt{\alpha^c}}\sqrt{\pi}\,\mathrm{erfc}\frac{(4n-2)R}{2\sqrt{\alpha^c t}}\right]$$
$$-(T_{\mathrm{EC1},i}-T_{\mathrm{EC2},i})\sum_{n=1}^{N}h^{2(n-1)}$$
$$\times\left[\sqrt{t}\exp\left(-\left[\frac{(4n-3)R}{2\sqrt{\alpha^c t}}\right]^2\right)\right.$$
$$\left.-\frac{(4n-3)R}{2\sqrt{\alpha^c}}\sqrt{\pi}\,\mathrm{erfc}\frac{(4n-3)R}{2\sqrt{\alpha^c t}}\right]$$
$$+(T_{\mathrm{EC1},i}-T_{\mathrm{SI},i})\sum_{n=1}^{N}h^{2(n-1)}$$
$$\times\left[\sqrt{t}\exp\left(-\left[\frac{(4n-4)R}{2\sqrt{\alpha^c t}}\right]^2\right)\right.$$
$$\left.\left.-\frac{(4n-4)R}{2\sqrt{\alpha^c}}\sqrt{\pi}\,\mathrm{erfc}\frac{(4n-4)R}{2\sqrt{\alpha^c t}}\right]\right\} \quad \text{(S.5)}$$